Active dust devils in Gusev crater, Mars: Observations from the Mars Exploration Rover Spirit

Ronald Greeley,[1] Patrick L. Whelley,[1] Raymond E. Arvidson,[2] Nathalie A. Cabrol,[3] Daniel J. Foley,[1] Brenda J. Franklin,[4] Paul G. Geissler,[5] Matthew P. Golombek,[4] Ruslan O. Kuzmin,[6] Geoffrey A. Landis,[7] Mark T. Lemmon,[8] Lynn D. V. Neakrase,[1] Steven W. Squyres,[9] and Shane D. Thompson[1,10]

Received 3 May 2006; revised 13 September 2006; accepted 27 September 2006; published 7 December 2006.

[1] A full dust devil "season" was observed from Spirit from 10 March 2005 (sol 421, first active dust devil observed) to 12 December 2005 (sol 691, last dust devil seen); this corresponds to the period L_s 173.2° to 339.5°, or the southern spring and summer on Mars. Thermal Emission Spectrometer data suggest a correlation between high surface temperatures and a positive thermal gradient with active dust devils in Gusev and that Spirit landed in the waning stages of a dust devil season as temperatures decreased. 533 active dust devils were observed, enabling new characterizations; they ranged in diameter from 2 to 276 m, with most in the range of 10–20 m in diameter, and occurred from about 0930 to 1630 hours local true solar time (with the maximum forming around 1300 hours) and a peak occurrence in southern late spring ($L_s \sim 250°$). Horizontal speeds of the dust devils ranged from <1 to 21 m/s, while vertical wind speeds within the dust devils ranged from 0.2 to 8.8 m/s. These data, when combined with estimates of the dust content within the dust devils, yield dust fluxes of 3.95×10^{-9} to 4.59^{-4} kg/m^2/s. Analysis of the dust devil frequency distribution over the inferred dust devil zone within Gusev crater yields ~50 active dust devils/km^2/sol, suggesting a dust loading into the atmosphere of ~19 kg/km^2/sol. This value is less than one tenth the estimates by Cantor et al. (2001) for regional dust storms on Mars.

Citation: Greeley, R., et al. (2006), Active dust devils in Gusev crater, Mars: Observations from the Mars Exploration Rover Spirit, *J. Geophys. Res.*, *111*, E12S09, doi:10.1029/2006JE002743.

1. Introduction and Background

[2] Solar insolation and heterogeneities in rock and particle distributions result in uneven surface heating, which generates rising, vortical columns of air, or "thermals." Thermals can develop over any terrain or surface on Earth or Mars, and are made visible as dust devils when they entrain dust particles in the vortex (Figure 1). *Sinclair* [1969, 1973] noted that the atmospheric structure within dust devils consists of a swirling vortex with vertical upward flow forming a "core" and lateral inflow of air near the bottom of the vortex. He also observed downward flow in the center of some dust devils. The tangential velocity profile of many dust devils approximates the Rankine vortex model [e.g., *Lugt*, 1983] in which the tangential velocity within the main core is proportional to the radius, and the tangential velocity in the outer vortex flow is proportional to the inverse of the radius.

[3] In our discussion of particles transported by dust devils, we refer to "granules" (grains 2000–4000 micrometers in diameter typically transported by surface creep or "reptation"), "sands" (grains 62 to 2000 micrometers in diameter transported mostly in saltation), and "dust" (fine-grained material <62 micrometers in diameter transported in suspension). Martian atmospheric dust is estimated to be a few micrometers in diameter [*Lemmon et al.*, 2004].

[4] Dust devils have been suggested as aeolian transport mechanisms on Mars by many workers, including *Neubauer* [1966], *Sagan and Pollack* [1969], *Sagan et al.* [1971], *Ryan and Luchich* [1983], and *Leovy* [2003]. The existence of Martian dust devils was confirmed by *Thomas and Gierasch* [1985], who discovered some 100 dust devils in Viking Orbiter (VO) images. These features were as large as 1 km across and extended a few kilometers above the

[1]School of Earth and Space Exploration, Arizona State University, Tempe, Arizona, USA.
[2]Department of Earth and Planetary Sciences, Washington University in St. Louis, St. Louis, Missouri, USA.
[3]NASA Ames Research Center, Moffett Field, California, USA.
[4]Jet Propulsion Laboratory, Pasadena, California, USA.
[5]Astrogeology Program, U.S. Geological Survey, Flagstaff, Arizona, USA.
[6]Vernadsky Institute, Russian Academy of Sciences, Moscow, Russia.
[7]NASA Glenn Research Center, Cleveland, Ohio, USA.
[8]Department of Atmospheric Sciences, Texas A&M University, College Station, Texas, USA.
[9]Department of Astronomy, Cornell University, Ithaca, New York, USA.
[10]Now at Department of Geological Sciences, University of Nevada at Reno, Reno, Nevada, USA.

0148-0227/06/2006JE002743

Figure 1. Dust devil in the Bolivian Altiplano at Laguna Blanca, showing typical morphology. Maximum height is about 100 m; the dust devil was moving from left to right. (Photo credit: 2004 Licancabur Expedition, NAI/SETI/NASA ARC/Stanford University.)

surface. More recently, *Edgett and Malin* [2000a, 2000b] found numerous dust devils, some as high as 6 km, from analyses of Mars Orbiter Camera (MOC) images. Similarly, *Biener et al.* [2002] identified dust devils as wide as several kilometers in MOC images. Smaller active dust devils (~20 m across) were also observed in high-resolution MOC images [*Edgett and Malin*, 2000a, 2000b], which left dark tracks, confirming earlier speculations based on VO images that some dark linear streaks on Mars result from the passage of vortices [*Grant and Schultz*, 1987]. The vortex column extends upward from the surface and can then be moved across the surface by the wind, leaving the track in its wake. Most Martian dust devil tracks are considered to result from the removal of bright dust from the surface exposing a relatively dark substrate. However, we also note that some tracks are bright relative to the surrounding surface, perhaps indicating that the entrainable particles are darker than the substrate. The discussion in this report is restricted to dark tracks, the most common type found on Mars and in Gusev crater.

[5] In general, Martian dust devil tracks vary from relatively straight paths, to curvilinear features, to looping patterns, depending on the nature and strength of surface winds affecting the vortex. Many tracks are only tens of meters across, although some are >250 m wide [*Fisher et al.*, 2005]. As outlined by *Edgett and Malin* [2000b], the patterns seem to be little affected by the terrain over which they pass, including craters, cratered terrain, and fields of sand dunes. This is in contradiction to some observations of terrestrial dust devil tracks [*Rossi*, 2002; *Rossi and Marinangeli*, 2004], which change form over some topographic features. Dark dust devil tracks are observed to fade over time, suggesting that the light-toned dust settles back to surface and eventually erases the albedo difference that marks the path of the dust devil [*Malin and Edgett*, 2001; *Balme et al.*, 2003].

[6] Active dust devils were also detected from landers on Mars. For example, the Mars Pathfinder (MPF) meteorology data suggest that numerous atmospheric vortices passed over the lander [*Schofield et al.*, 1997; *Ringrose and Zarnecki*, 2002; *Ferri et al.*, 2003], during which pressure excursions of 1–5 Pa were measured, equating to ~0.2–1.0 percent of the ambient pressure. In addition, the MPF camera captured at least five active dust devils, which developed in rapid succession [*Smith and Lemmon*, 1999; *Metzger et al.*, 1998a, 1998b, 2000; *Ferri et al.*, 2003]. These dust devils occurred during a relatively calm period on Mars (L_s = 143°), when maximum surface winds were no more than about ~10 m/s [*Schofield et al.*, 1997], far less than boundary-layer threshold for the movement of sand and dust, and strongly suggesting that dust devils are an effective mechanism for particle entrainment [*Metzger*, 2001; *Greeley et al.*, 2003]. More recently, *Ringrose et al.* [2003] reanalyzed Viking Lander (VL) data and concluded that VL-2 experienced some 38 possible dust devils.

[7] The operation of the Mars Exploration Rovers (MER) with the Athena science payload [*Squyres et al.*, 2003; *Squyres and the Athena Science Team*, 2004], coupled with concurrent observations from orbit, provide new insight into the characteristics of dust devils. For example, the Spirit landing site (Columbia Memorial Station, or CMS) in Gusev crater appears to have been crossed by numerous dust devils leaving dark tracks, some of which formed a few months before the landing on 4 January 2004. Spirit landed in one fresh track, as seen in MOC images, and then crossed out of the track in the traverse to the Columbia Hills. Microscopic Imager (MI) [*Herkenhoff et al.*, 2004] data showed that the sand grains in the track zone are relatively free of finer, higher albedo material (considered to be dust), while the sands outside the track zone are dusty [*Greeley et al.*, 2004; *Foley et al.*, 2005; *Metzger*, 2005]. This confirms earlier models that the tracks result from the passage of dust devils that sweep the surface free of fine particles, exposing a surface that has a lower albedo than the bright dust. It appears that the particles entrained by dust devils are derived from a relatively thin layer of dust that mantles coarser, darker particles.

[8] In the extended phase of Spirit operations, the rover traversed into the Columbia Hills to the top of Husband Hill, some 110 m above the landing site on the crater floor. Beginning on 10 March 2005 (sol 421 (L_s 173.2°), or 421 Martian days after landing), active dust devils were observed on the plains from the perspective afforded from the hills (Figure 2). In the ensuing 270 sols (until sol 691 (L_s 339.5°)), some 533 active dust devils were imaged by Spirit. This period represents the spring and summer seasons in the southern hemisphere. In addition to the MI, the Athena

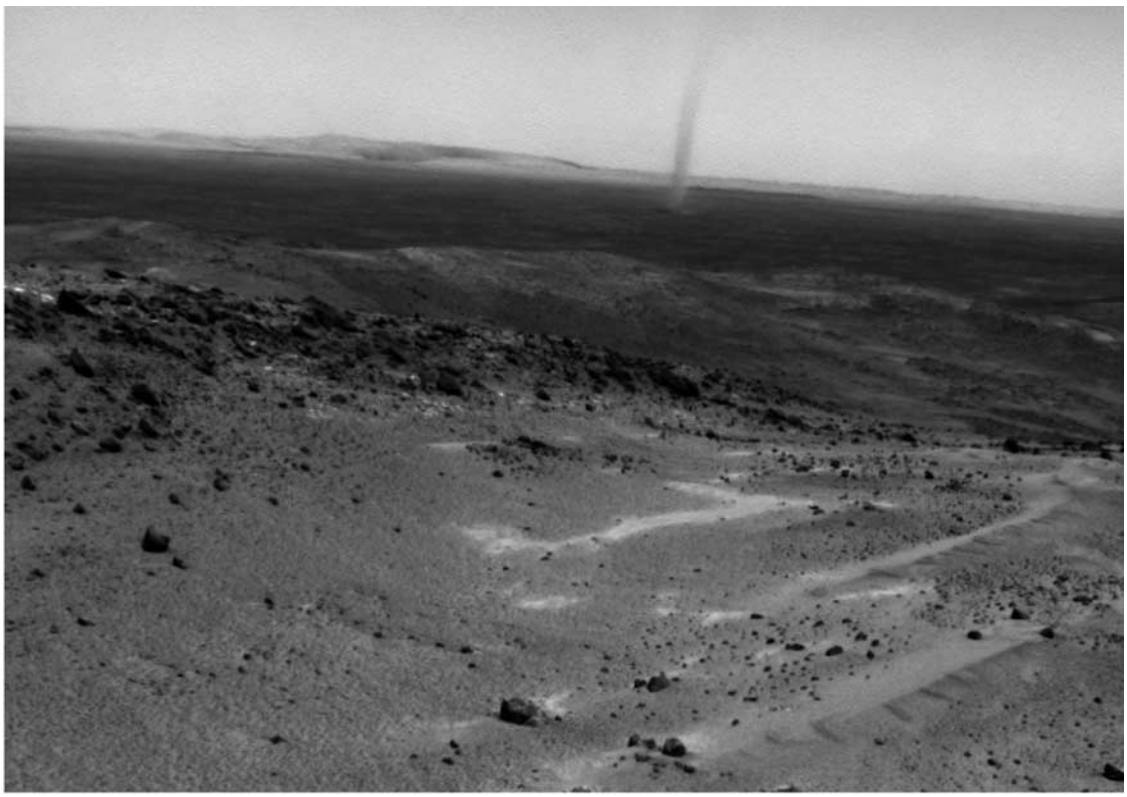

Figure 2. Dust devil on the floor of Gusev crater, imaged on sol 616 by the Spirit Navcam (image 2N181053592EFFAEOTP0607L0M1) from the Columbia Hills. This dust devil is about 1 km from the rover and is estimated to be at least 95 m high. The image was enhanced to increase contrast.

instrument suite on Spirit [*Squyres et al.*, 2003] includes three imaging systems, the Panoramic Camera (Pancam) [*Bell and the Athena Science Team*, 2004] and the Navigation Camera (Navcam), both of which are mounted on a mast and view the terrain from a height of about 1.5 m, and the Hazard Cameras (Hazcams), fixed to the front and rear of the rover chassis about 0.5 m above the ground at the front and the rear of the rover [*Maki et al.*, 2003]. All three camera systems acquire stereoscopic images. Pancam is a multispectral imager, while the others are panchromatic. Image formats for all three imaging systems are 1024–1024 pixels. Fields of view are 16.8–16.8° for Pancam, 45–45° for Navcam, and 120–120° for Hazcam. Navcam was the primary instrument for our study of active dust devils because of its combination of wide field of view and the ability to point it in a desired direction each sol. Pancam and Hazcam images were not typically used for planned dust devil observations, although serendipitous observations of dust devils were made in these images. There were also many serendipitous detections of dust devils in Navcam images acquired for other purposes.

[9] After the initial discovery of the first dust devils in Spirit images and recognizing that they were likely to be a recurring phenomenon, we designed and implemented 21-frame Navcam ''dust devil movie'' sequences with the hope of observing dust devils in motion. During the time when dust devils were common, Spirit was high on Husband Hill, with a good view over the plains of Gusev crater, particularly to the west. A typical Navcam dust devil movie was targeted from this vantage point, usually in the middle of the day when rover solar power was most available and dust devils most likely to be present. Because dust devils are seen best at or near the horizon, dust devil movie images were typically targeted to include the horizon, and ''subframed'' to be 1024 pixels wide but only 256 pixels high. Data volume was a concern for products such as dust devil movies that can generate many megabits of image data, and the reduced data volume yielded by subframing allowed more images to be acquired. In some instances data volume concerns were addressed further by first downlinking highly-reduced ''thumbnail'' images sufficient to reveal whether or not dust devils were imaged. If no evidence of dust devils was seen in the thumbnail images, the full-resolution images could be deleted onboard the rover, rather than downlinked. Because downlinked data volume (rather than onboard storage) was often the greatest concern, this approach further increased the number of dust devil movies that could be acquired.

[10] Dust devils could only be seen in the directions and at the times when images were acquired. Thus, rather than conducting a systematic or random sampling for all times of day and all azimuths, we chose the times and azimuths that we considered to be most suitable for imaging large numbers of dust devils. We did this (in part) as an observational choice, but also because of practical issues such as availability of power and ease of command sequencing.

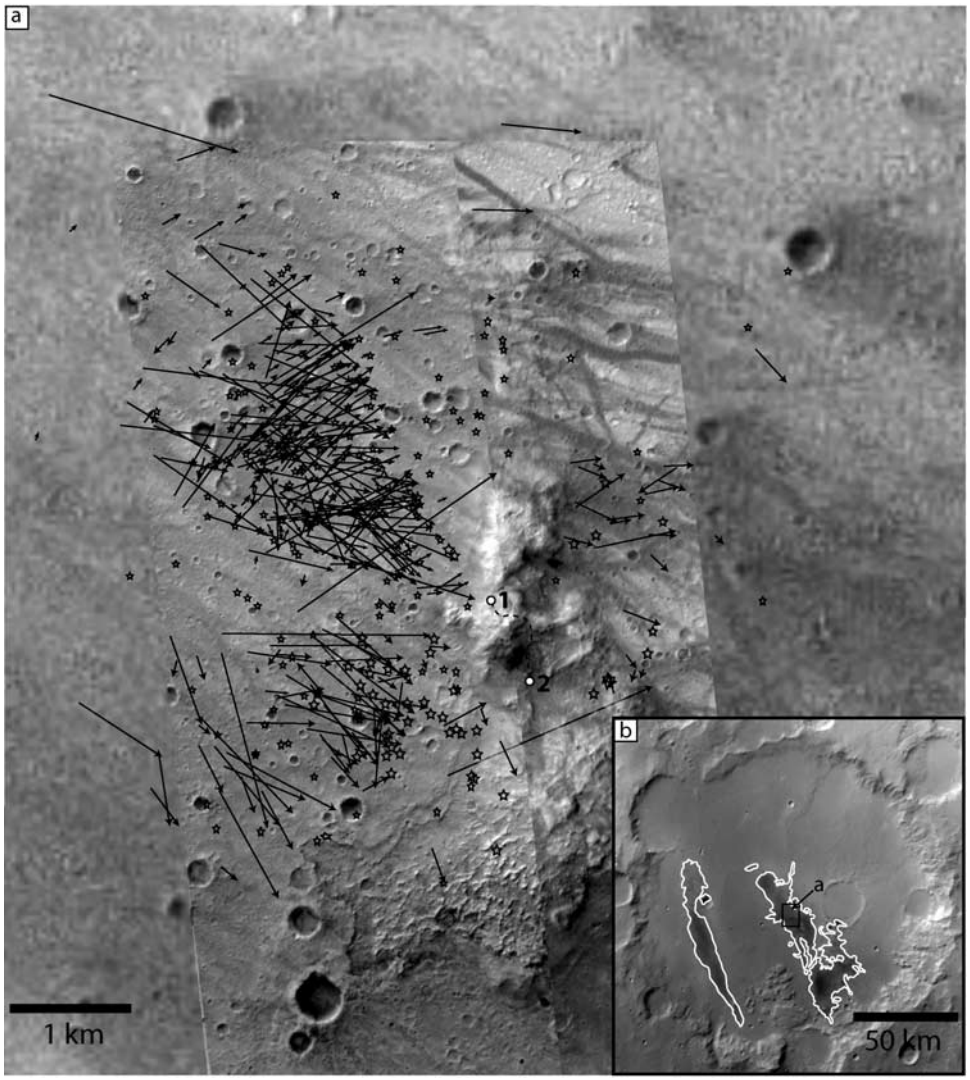

Figure 3. (a) Mosaic of orbiter images of the Columbia Hills showing the positions of the rover (1, 2) between which most of the observations of active dust devils were made. Black lines and arrows show the tracks and directions of active dust devils; stars indicate single observations of active dust devils. Dark linear patterns on the surface are inferred to be tracks left by the passage of dust devils. (b) Gusev crater showing the location of Figure 3a, and the two prominent low-albedo zones on the crater floor. (c) Diagrams showing the viewing geometry from the rover during the period of active dust devils as a function of sol and L_s, as the rover moved from position 1 to position 2 (see Figure 3a).

Moreover, the range of azimuths available for far-horizon imaging changed during the mission as the rover moved relative to the topographic features around it. Thus, while the observation strategy was effective in leading to many dust devil observations, it also unavoidably led to certain biases in our data set that must be kept in mind when considering the results.

[11] Figures 3a and 3b show the location of the observed dust devils and the approximate paths for those that were seen in more than one image. Figure 3c shows the general viewing geometry of the plains from Spirit during the active dust devil period. Figure 3a is a mosaic of MOC images used to locate individual dust devils through a comparison of surface landmarks, such as craters, seen from both orbit and the rover. Typically, 2 to 4 landmarks were identified around each dust devil and were used to define an ellipse centered on the inferred location of the dust devil, with the ellipse size indicating the uncertainty in location. Uncertainties range from 15 to 2500 m, with dust devils farthest from the rover typically having the greatest uncertainty in location because of the oblique viewing perspective. Vectors of dust devil movement were based on the centers of the ellipses for the first and last image in which the same dust devil was seen (Figures 4b and 4c).

[12] The light-colored dust devils are most visible against a comparatively darker surface. Image enhancement, such as "stretching," allowed the part of the dust devil extending above the horizon to be visible. Figure 5 shows a dust devil from sol 486 in a Navcam image before and after image processing, including contrast enhancement (Figure 5b).

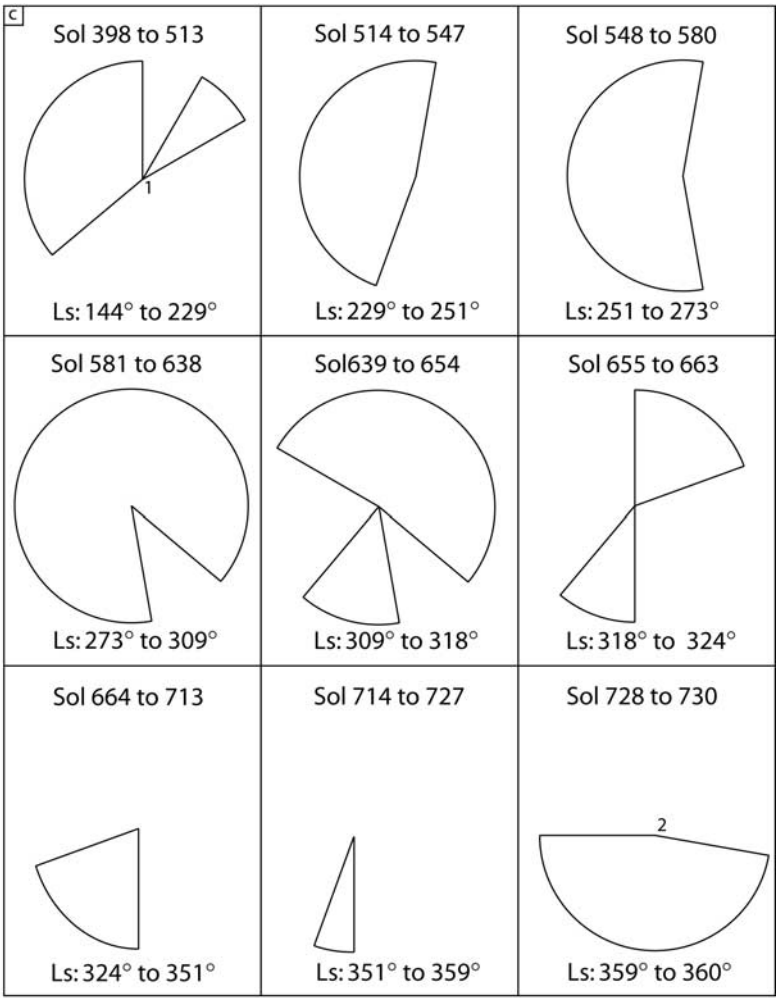

Figure 3. (continued)

The dust visible above the horizon is darker than the background sky. When individual dust devils were imaged in the dust devil movies (Figure 6), directions and speeds of motion were determined from the estimated distance traversed and the time intervals between frames. In a few cases, the formation, evolution, and dissipation of individual dust devils were recorded. The time-sequenced images, coupled with determinations of dust optical opacities within the vortexes, allowed estimates of the dust flux.

[13] The Spirit data provide unprecedented insight into the formation and evolution of dust devils and their role in Martian aeolian processes. In this report we describe the morphology and characteristics of the active dust devils in Gusev crater compared to terrestrial dust devils and those seen elsewhere on Mars, derive information on the fluxes of dust within the Gusev dust devils, and discuss the implications for the dust loading into the atmosphere.

2. Gusev Dust Devils

2.1. Morphology

[14] Dust devils on Earth typically form clouds of dust that taper slightly toward the sky and become diffuse with height, an indication of dust suspension and dissipation into the atmosphere. A relatively clear zone is seen in the center of some columns, which suggests the presence of a core that contains less dust, and perhaps lower vortex speed. Some terrestrial dust devils also have a "skirt" close to the ground that is wider than the main column of dust. This skirt typically consists of larger particles, such as sand and clumps of dust, which are ejected from the column by radially-directed winds (or centripetal winds in the vortex) and which are too large to be carried aloft in suspension. As some of these grains return to the surface, they can continue to move short distances in saltation, setting other grains into motion locally. The net result is a flurry of surface activity in which grains are jostled and moved short distances in a zone that can be 2–4 times wider than the main dust devil column.

[15] Although rare, some dust devils in Gusev crater show an observable near-surface skirt (Figure 7); however, most lack this feature, suggesting that either granules or sand grains are not present on the surface, or that most of the grains are immobile at the wind speeds within the dust devils. MI data from Spirit obtained on the traverse to the Columbia Hills show the presence of sands and granules in surface soil deposits [*Herkenhoff et al.*, 2004]. Thus it would appear that the sands are relatively immobile, a conclusion consistent with the interpretation of *Greeley et*

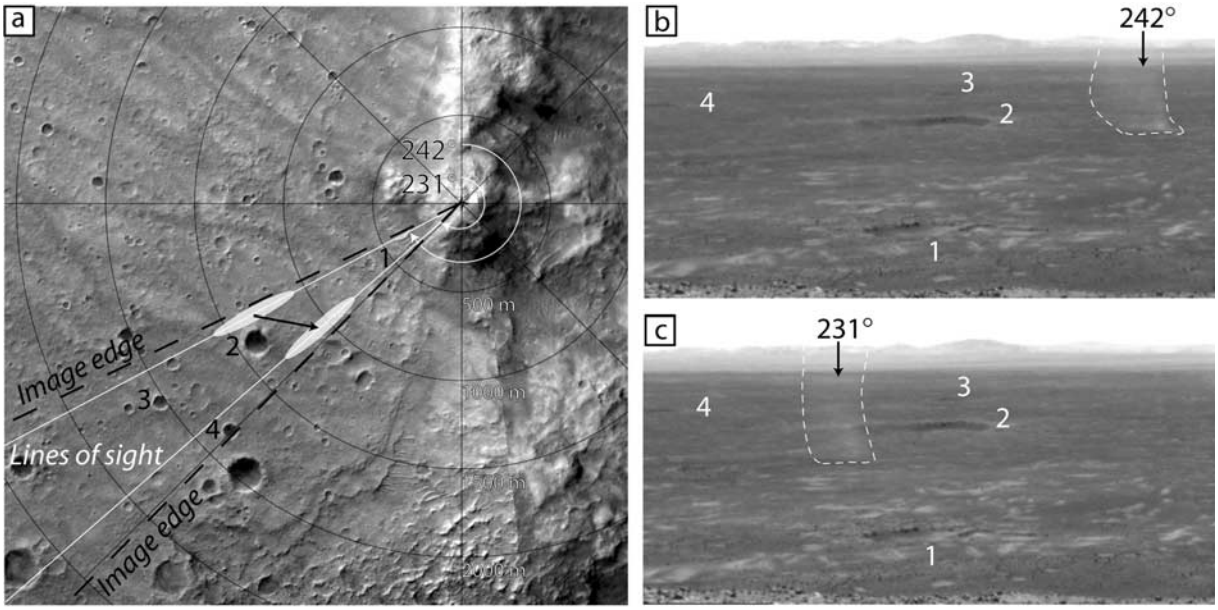

Figure 4. Illustration of the method used to estimate the location of dust devils, based on matching surface features seen from orbit with those seen from the rover and their azimuths from the rover (Figures 3b and 3c). The white ellipses indicate the uncertainty in location; the black arrow indicates the estimated travel distance and direction from which wind speed was estimated, using the framing rate between sequential images. (b) Image 2N177056615ESFADAEP1560L0M1 and (c) image 2N177056656ESFADAEP1560L0M1 are two frames showing the same dust devil. The white numbers in Figures 4b and 4c correspond to the black numbers in Figure 4a. This dust devil was observed on sol 571 and traveled 300 m in 41 seconds in an ESE direction between Figures 4b and 4c.

al. [2004, 2005], based on the presence of dust within the sand deposits which suggests a general lack of active saltation which would be expected to cleanse the sands of dust. However, at least some active sand saltation is suggested within the Columbia Hills, as indicated by the accumulation of sand grains on the top of the rover deck at about the time that the active dust devils were first observed [*Greeley et al.*, 2006; *Landis et al.*, 2006].

[16] Terrestrial dust devils move across surfaces by wind in paths that can be relatively linear, curved, or even curlicue, or looping. In the waning stages, they often loose the well-defined vortex structure and break up into diffuse clouds of dust. Similarly, many of the dust devils at Gusev become diffuse as the vortex structure degrades.

[17] Dust devils observed from Spirit range in diameter from 2 to 276 m, with most in the 10 to 20 m range (Figure 8a), for a mode of 12 m. This peak range is somewhat larger than seen on Earth where the mean diameter is about 7 m (see review by *Balme and Greeley* [2006]). Smaller dust devils are probably under-reported on Earth, however, and the same is almost certainly true on Mars. Martian dust devil diameters do not show any clear trend with respect to time of day (Figure 8b). However, diameters of the largest dust devils observed on a daily basis were greatest toward the middle of the period of observation (sol 421 (L_s 173.2°) to sol 691 (L_s 339.5°)), peaking around sol 540 (L_s 246.75°; Figure 8c). The heights of most of the dust devils seen from Spirit cannot be determined because most images do not show the full structure. However, 44 were seen in full, indicating a height range of 9 to 361 m compared to terrestrial dust devils which range from 1 to 2500 m in height, with most being 3–50 m high [*Balme and Greeley*, 2006]. One particularly tall dust devil was seen from Spirit where the top of the column was "truncated" by the top edge of the image, indicating a minimum height of 848 m. The heights of dust devils seen on Earth and on Mars from Spirit are considerably lower than those seen on Mars from orbit, which range up to 8500 m [*Fisher et al.*, 2005]. This suggests that either those in Gusev crater are shorter for some reason, or that the sampling of dust devil heights by the two observation techniques (i.e., from orbit and from the ground) is statistically different. Given the substantial difference in viewing geometry and the paucity of images acquired from the ground that show the full height of dust devils, we favor the latter explanation.

[18] Viewed in profile, many terrestrial dust devil columns form a curving arc upward, or appear to "lean" (Figure 9). This is attributed to deformation in the prevailing downwind direction and a reflection of the boundary layer shear, in which wind speeds increase with height causing a tilt in the downwind direction. A similar "leaning" or curving profile is seen in some of the Gusev dust devils (Figures 4b and 4c), which enables the local wind directions to be inferred, as described below.

2.2. Occurrence

[19] Figure 3b shows that the dust devils observed from Spirit occur in a prominent low-albedo zone on the floor of Gusev crater, as seen in moderate-resolution images taken from orbit. The low-albedo zone is attributed at least partly

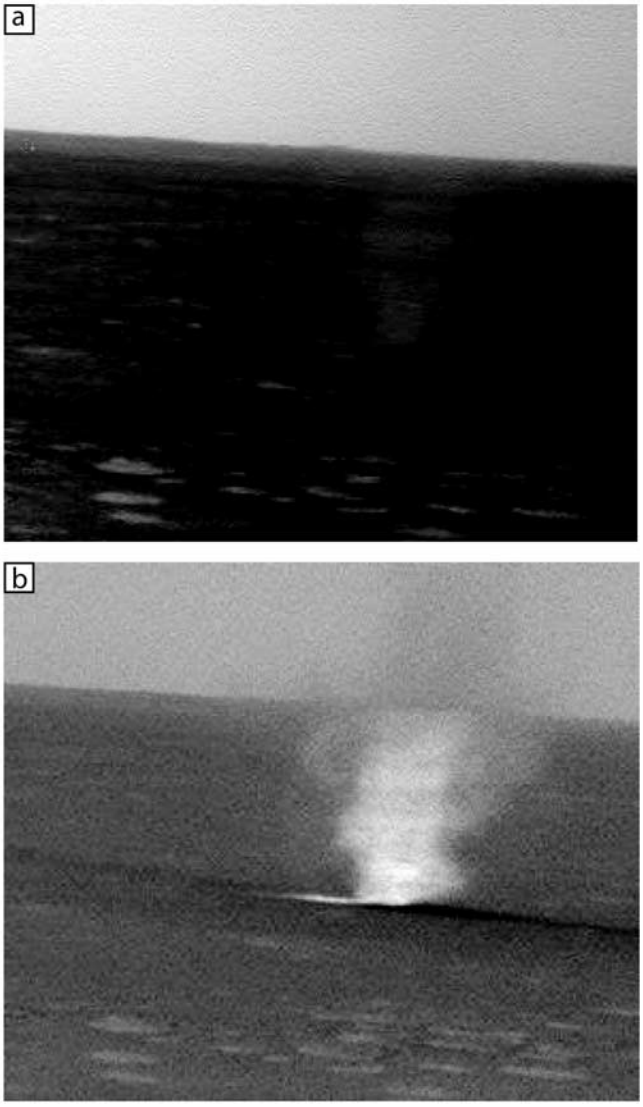

Figure 5. (a) Navcam image from Spirit, sol 486, taken at 1155 local solar time (image 2N169504452ESFAAB2-P1560L0M1) showing dust devil as imaged and (b) after image enhancement to emphasize detail.

to the presence of numerous dark, linear and curvilinear streaks formed by the passage of dust devils over the surface. Because these features were well known prior to the landing of Spirit on 4 January 2004 (sol 1 (L_s 327.7°)), it was expected that active dust devils would be common early in mission operations because the landing occurred during late summer when dust devils were thought to be frequent. Despite searches for active dust devils using rover images, none were observed until sol 421 (L_s 173°), more than one Earth year after landing. As shown in Figure 10, frequency of dust devils increased to a peak of 0.11 per km^2, centered at sol 555 (L_s 256.7°). The period of active dust devils in Gusev crater covers southern spring and each summer.

[20] Observed Gusev dust devils occurred from about 0930 to 1630 hours local true solar time (LST), with the maximum seen around 1300 hours (Figure 11). Undoubtedly some bias is present in this distribution because imaging for dust devil detection and other purposes was particularly common during the middle of the day. Note that the image coverage is indicated in Figures 10 and 11 to provide a qualitative assessment of the potential bias. A total of 349 dust devils were studied to determine their "lifetimes," of which 70 were seen in full cycle from initiation to termination. Values ranged from 21 to 687 seconds. The remaining 279 represent either dust devils that were already in action at the start of the Navcam sequence, or that began during the sequence and were still active in the last frame; in both of these cases, the durations represent minimum lifetimes, which ranged from 20 to 1936 seconds. The mean of all the observations is 170 seconds. These values are consistent with terrestrial dust devils, which occur between 1000 and 1730 hours and typically last for a few minutes. However, *Ives* [1947] noted that some dust devils in Utah lasted as long as 7 hours, traveling ~60 km across the surface, and suggested an empirical relationship of 1 hour duration for every 300 m of height.

2.3. Speeds

[21] Repeat imaging of dust devils over time enables calculation of horizontal speeds, as well as estimations of vertical speeds within the vortexes. As shown in Figure 12, horizontal wind speeds ranged from <1 to 21 m/s. *Balme and Greeley* [2006] reviewed field measurements of terrestrial dust devils and found a range of 5–10 m/s with peak values of about 20 m/s. Figure 13 shows the wind speeds as a function of sol during the period observed. It should be noted that there is no true "minimum speed" within the available data. For example, a dust devil observed in repeat images moving directly toward the camera would appear to be motionless if it were moving directly toward the camera, although it might appear to be larger.

[22] Average vertical speeds of dust lifted in dust devil columns were estimated for the first time on Mars from Spirit Navcam image sequences. Concentrations of dust seen in the images as bright zones (inferred to be "clots" of dust) and changes in dust devil height could be followed in some image sequences. The vertical component of their changes in position were measured, which, combined with the time between frames, enabled the vertical speeds to be estimated. Results for 67 dust devils range from 0.2 to 8.8 m/s, with an average vertical speed of 1.8 m/s (Figure 14). Inconsistencies between observers in estimates of vertical speed (due to uncertainties in the distance between the dust devil and the rover (Figure 4), and subjective observer error) are, on average, 0.7 standard deviations, based on two analysts who examined the images independently. It should also be noted that it is not possible to determine the precise geometry of the "clot" locations within the three dimensions of the dust column, and that the estimates are therefore minimum values. The 1.8 m/s value compares with measured vertical speeds of dust devils on Earth of 3 to 7 m/s [*Metzger*, 1999], and is within the range of previous estimates for Mars. For example, *Metzger et al.* [1999] assumed the 7 m/s from terrestrial dust devils in his application to Mars, while *Rennó et al.* [1998, 2000] modeled the maximum dust devil vertical velocity to be 15 m/s and *Ferri et al.* [2003] used a value

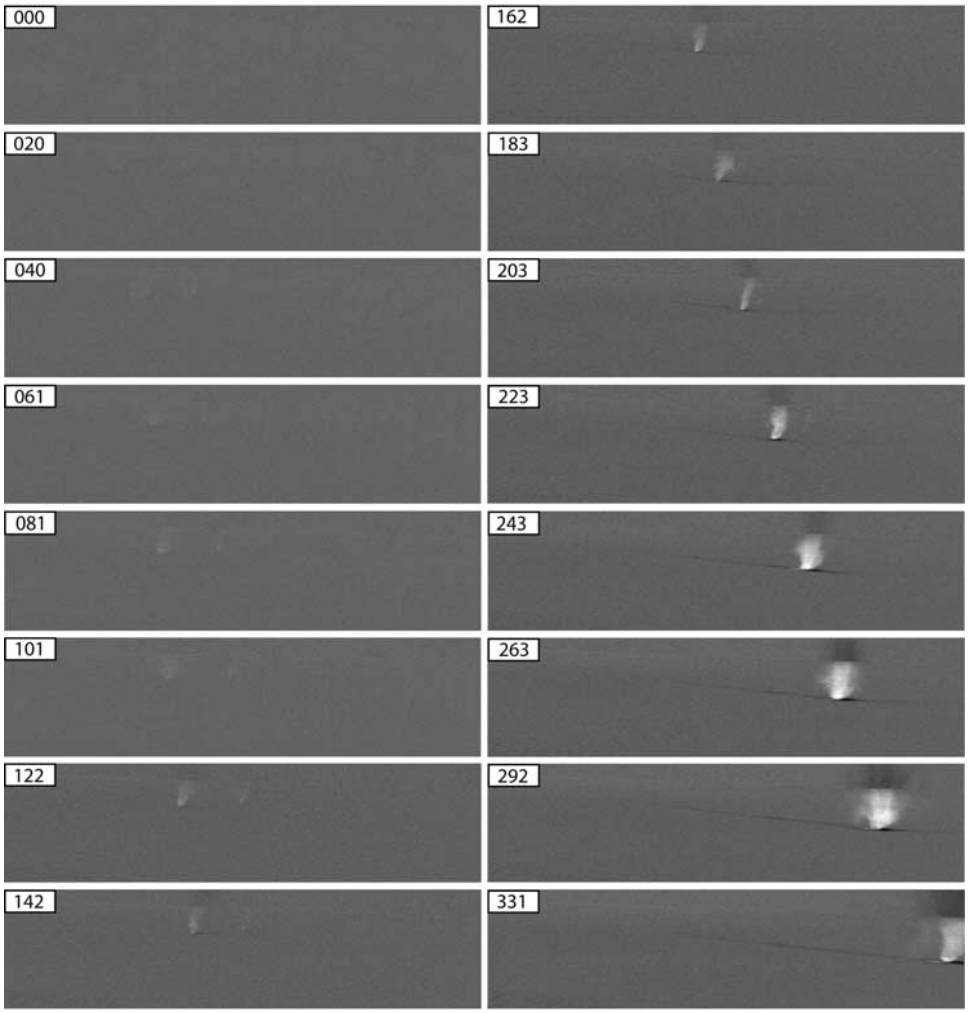

Figure 6. Typical sequence of Navcam images (sol 486) used in the analysis of active dust devils. Numbers in upper left corner indicate elapsed time in seconds. The images were enhanced for analysis of the dust devil. Note the dark streak left in the wake of the dust devil as it moved left to right across the field of view (times 183–331 s). The shadow cast by the column of dust is also seen (e.g., time 243 s). The dark zone at the top of the dust devil column in time frames 203–331 is above the local horizon in which the dust is visible as darker than the background sky. Sequence with image 2N169504171ES-FAAB2P1560L0M1.

for Mars of 20 m/s based on modeled thermal updraft velocities.

2.4. Inferred Wind Directions

[23] Dust devils that were imaged more than once were tracked to infer their directions of motion (Figure 3a). Figure 15 presents rose diagrams showing the directions of movement for 326 dust devils from sol 421 to 575 (L_s 173° to 270°, or southern spring). The prevailing direction is toward the northeast in the spring (Figure 15a). Note, however, that there is a difference in the strength of the winds in the spring, in which the direction of the strongest winds is toward the southeast (Figure 15c). In the summer, the directions are less consistent (Figure 15b) but the prevailing trend is toward the southeast, which correlates with noon to afternoon winds in the area predicted by the Mars Regional Atmospheric Modeling System (MRAMS) [*Rafkin et al.*, 2001; *Rafkin and Michaels*, 2003]. This direction is also consistent with the orientations of various wind-related features, such as small dunes and ventifacts, imaged by Spirit on the traverse to the Columbia Hills [*Greeley et al.*, 2004, 2005]. Moreover, MRAMS predicts wind speeds of 1 to 3 m/s at a height of 2 m, consistent with the dust devil horizontal speeds observed in Gusev crater (Figure 12). While MRAMS predicts a consistent wind direction from 900 to 1600 hours, wind speed is predicted to increase late in the day. For example, most of the dust devils that moved faster than 2 m/s occurred after 1300 hours (Figure 12), consistent with the MRAMS predictions.

3. Determination of Dust Flux From Image Data

[24] The relative dust opacities within dust devils are derived from image pixel intensities. The brightness of a pixel of the background scene viewed on a line of sight

Figure 7. Dust devil imaged by Navcam (image 2N1831-83331ESFAI00P1560L0M1) on sol 640, showing well-developed skirt (the broad, bright zone beneath the column). Image has been contrast stretched to enhance detail but is not very sharp because the dust devil is more than 2.5 km from the rover.

passing through the dust devil is equal to the brightness of the scene, as diminished by the loss of intensity of the beam by passage through the optical depth of the dust devil, plus the brightness of the scattered light from the dust devil. From the principle of reciprocity, these two components must be added with weighting factors equal to unity (i.e., all lines of sight must either terminate on the background scene, or terminate or be scattered by the dust in the dust devil). The decrease in intensity of light from the background pixel viewed through the dust devil can be calculated from Beer's law:

$$I = I_g e^{-\tau_d}, \tag{1}$$

in which I is the observed intensity, I_g is the initial intensity (unattenuated), τ_d is the opacity of the dust raised by the dust devil. Note that the factor I_g incorporates the effect of all atmospheric dust on the line of sight other than the dust in the dust devil.

[25] To determine the dust opacity of a path through the dust devil, six intensities were measured: the brightness of the sky near the dust devil above the horizon (I_s), the initial intensity (I_g) on the ground near the dust devil, and four points through the dust devil (I_d). Calibration points I_s and I_g taken outside the dust devil were obtained from the leading (downwind) side of the dust devil to prevent contamination from lingering lofted dust.

[26] We assume that the optical properties of the dust incorporated into the dust devil are similar to the optical properties of the dust suspended in the atmosphere and that the brightness of the sky, I_s, measured at the same elevation and azimuth as the dust devil, can be used as a value for the brightness of light scattered from a dust devil of arbitrarily high optical opacity. Thus, since the two weighting factors must sum to unity, the intensity of the line of sight passing through the dust devil (I_d) is

$$I_d = (e^{-\tau_d})I_g + (1 - e^{-\tau_d})I_s = I_s + (I_g - I_s)e^{-\tau_d}. \tag{2}$$

Thus dust devil opacity (τ_d) is determined as

$$\tau_d = -\ln\left(\frac{I_d - I_s}{I_g - I_s}\right) = \ln\left(\frac{I_g - I_s}{I_d - I_s}\right). \tag{3}$$

Of the 348 Gusev dust devils for which opacity determinations were made, values of τ_d ranged from 0.01 to 2.64 (with a mean value of 0.14), which were used for flux determinations. Once τ_d was determined, it was related to the line-of-sight dust content in the dust devil. The dust content, δ, is calculated by relating the τ_d to values based on previous tau measurements, estimates of background dust concentration from Pathfinder, and the dust size distribution estimated by *Tomasko et al.* [1999], *Metzger et al.* [1999], and *Ferri et al.* [2003].

$$\delta = (\tau_d)(1.4 \times 10^{-3})\left[\mathrm{kg/m^2}\right] \tag{4}$$

(Note that, since the particle mass is proportional to particle diameter cubed, while optical scattering is proportional to the cross sectional area of the particle, this relationship will underestimate the dust mass if the average dust particle in the dust devil is larger than the average particle in the sky.)

[27] Dust concentration in the dust devil (d) is related to the dust content and the diameter of the dust devil as

$$d = \delta / L \tag{5}$$

and thus is related to dust opacity as

$$d = \left(\frac{\tau_d}{L}\right)(1.4 \times 10^{-3}). \tag{6}$$

The dust concentration enables the calculation of dust flux (Q_d, in kg/m^2/s) from the surface using an estimate of the vertical velocity (u_z)

$$Q_d = u_z d = u_z \frac{\tau_d}{L}(1.4 \times 10^{-3}). \tag{7}$$

In previous studies of the MPF dust devils, vertical velocities were based on typical terrestrial values (~7 m/s [*Metzger et al.*, 1999]) or typical thermal updraft velocities (~20 m/s [*Ferri et al.*, 2003]). As noted above, some MER dust devil movie sequences imaged clots of material that could be tracked from frame to frame allowing vertical speeds to be measured. Vertical speeds in Gusev crater ranged from 0.2 to 8.8 m/s with a mean of 1.8 m/s, which was used in our flux estimates. Of the total 330 observations

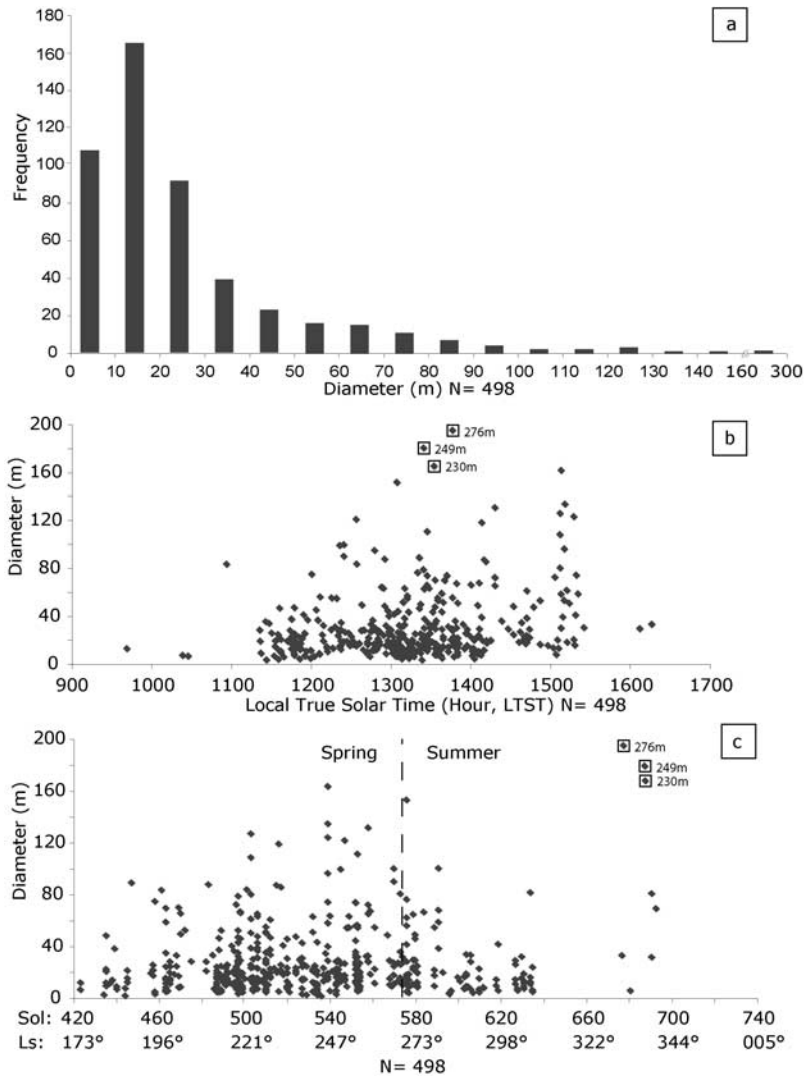

Figure 8. Analysis of dust devil diameters from a sampling of 498 cases: (a) size-frequency distribution, (b) diameter as a function of time of day, and (c) diameter as a function of sol and L_s covering the entire period of active dust devils. Exceptionally large dust devils are shown in Figures 8b and 8c as "boxed" values on the graphs.

for which the necessary data are available, the upward flux of individual dust devils ranged from 3.95 10^{-9} to 4.59 10^{-4} kg/m^2/s, with a mean value of 2.07 10^{-5} kg/m^2/s per dust devil.

4. Discussion and Conclusions

[28] Even before the landing of Spirit, the floor of Gusev crater was suspected to be a site of active aeolian processes, including dust devils, given the occurrence of wind streaks and inferred dust devil tracks. Two low-albedo patterns stretch north northwest across the crater floor from the mouth of Ma'adim Vallis, covering an area of some 3000 km^2 (Figure 3b). When viewed in high resolution (Figure 3a), this zone consists primarily of dust devil tracks where the active dust devils were observed from Spirit.

[29] Because Spirit landed in the southern hemisphere summer, active dust devils were widely expected to be observed early in the mission, yet none were seen until sol 421 and this result has posed a puzzle. Figure 16 provides some insight into the problem. Thermal Emission Spectrometer data (TES) [*Christensen et al.*, 2001] for about three Martian years were analyzed and the daytime (typically 1400 hours local time) temperatures were obtained for part of the floor of Gusev crater. The area covered is 14.5 to 15°S and 184 to 185°W, which includes CMS, Spirit's traverse, the Columbia Hills, and the area in which the active dust devils were observed. The results show that there is a correlation between the formation of dust devils and a rise in temperature. Such a correlation would be expected, given the role of surface temperature in the formation of dust devils on Earth. Note also that as the temperature stabilizes at about 275 K, the frequency of active dust devils decreases, showing that the thermal gradient is important, as well as a high temperature; this, too, would be expected, as

Figure 9. Dust devil near Eloy, Arizona, showing the "leaning" morphology, which indicates the direction of travel from the left toward the right. (Photograph by L. Neakrase, July 2005.)

vortexes are generated by unstable thermal conditions on the surface, and was predicted to be an important factor by *Rennó et al.* [1998, 2000]. Diurnal timing of dust devil activity is consistent with the period of maximum heat flux calculated from Viking 1 meteorological measurements [*Sutton et al.*, 1978] and Pathfinder observed dust devil frequency of occurrence [*Murphy and Nelli*, 2002]. Also shown on Figure 16 is the time of the Spirit landing. We suggest that the landing occurred in the waning stages of the dust devil season, which occurred with decreasing surface temperatures.

[30] On the basis of the observations reported above, we can now estimate the total dust that might have been lifted into the atmosphere from the low-albedo zone of Gusev crater during one full Martian year. Because the full area was not observed constantly, we must extrapolate the observations in both space and time. The primary data set used for this purpose consists of Navcam image sequences, which provide consistent observation areas and sequential frames with documented timing intervals. The observable area from Spirit forms a "doughnut" shaped zone with an inner radius of 500 m and an outer radius of 3500 m, giving a total surface area of 37.68 km^2. Each Navcam sequence covers an area of 4.71 km^2, or 1/8 of the total area of observations. During one full Martian year (L_s 0° to 360°), active dust devils were observed from L_s 173.2° to 339.5° (southern spring and summer) for 270 sols. However, Navcam sequences were taken for only 236 sols, and this is the value used for our statistical analysis. Most dust devils occur from 0930 to 1630 hours (midmorning to late afternoon), or 25,200 seconds. Thus the total duration of the dust devil season is 5,947,200 s (for the 236 sols of observations). Navcam 21-frame sequences range in duration from 7 to 20 min (420 to 800 s), depending on the framing rate, which is governed by other rover activities and resources. The sequences were spread throughout the day, with significant time intervals without imaging. A total time of 37,109 s was covered by all of the relevant Navcam sequences, which results in a factor of 160 for interpolating observations for the dust devil period.

[31] Thus the extrapolation of the active dust devils observed in the Navcam sequences over the total area and time is 351 dust devils (observed in the Navcam images) × 8 (area factor) × 160 (time factor) = 449,280. This number represents the total inferred dust devils, if

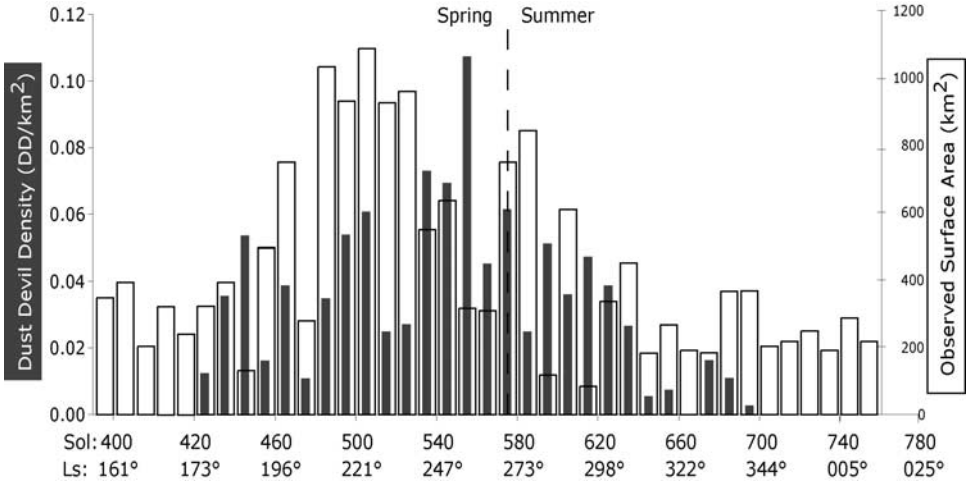

Figure 10. Density of active dust devils as a function of sol and L_s derived from observations over the floor of Gusev crater. Also shown is the cumulative area "sampled" by images during the entire period of observations.

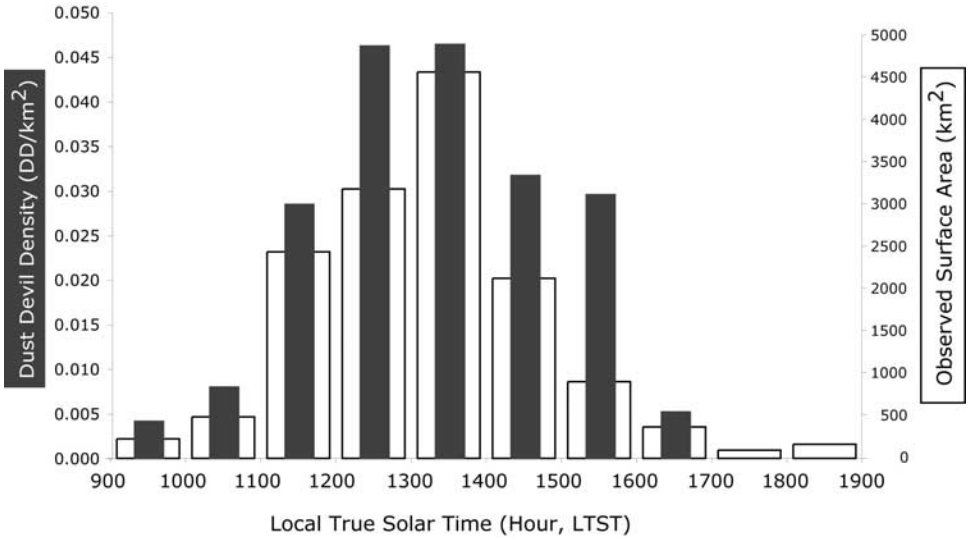

Figure 11. Density of active dust devils as a function of local time. Also shown is the cumulative area "sampled" by images during the entire period of observations.

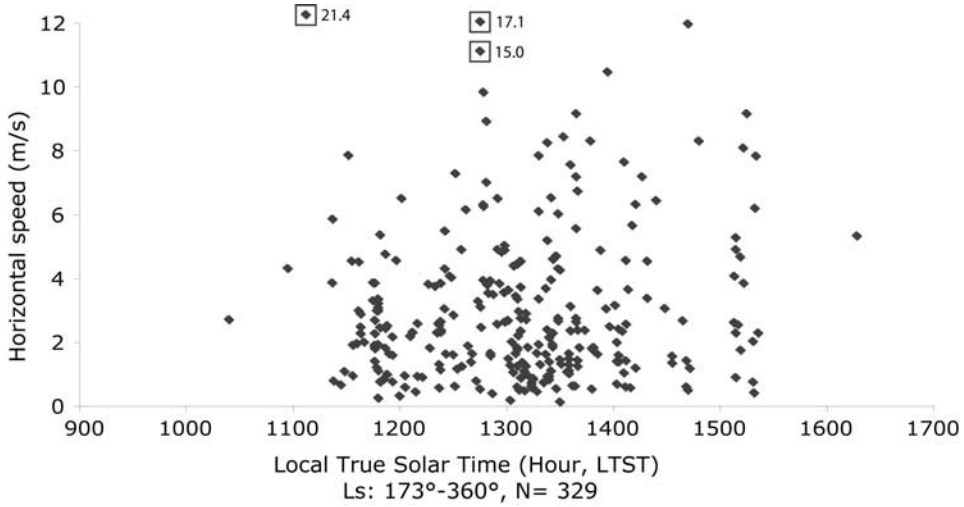

Figure 12. Horizontal speeds of 329 active dust devils as a function of local time. "Boxed" values indicate dust devils that plot off-scale.

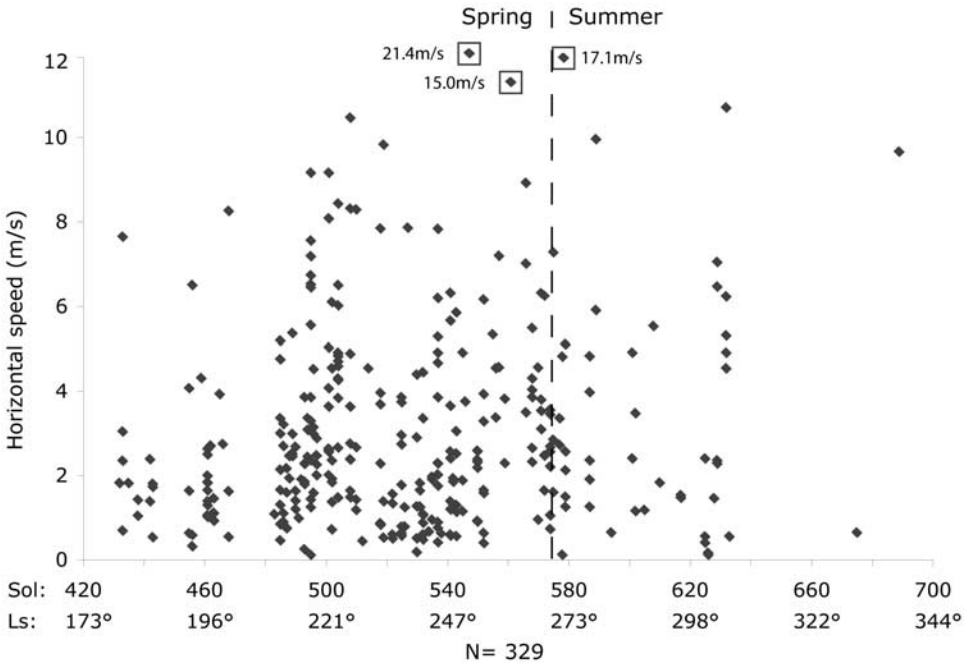

Figure 13. Horizontal speeds of 329 active dust devils as a function of sol and L_s. "Boxed" values indicate dust devils that plot off-scale.

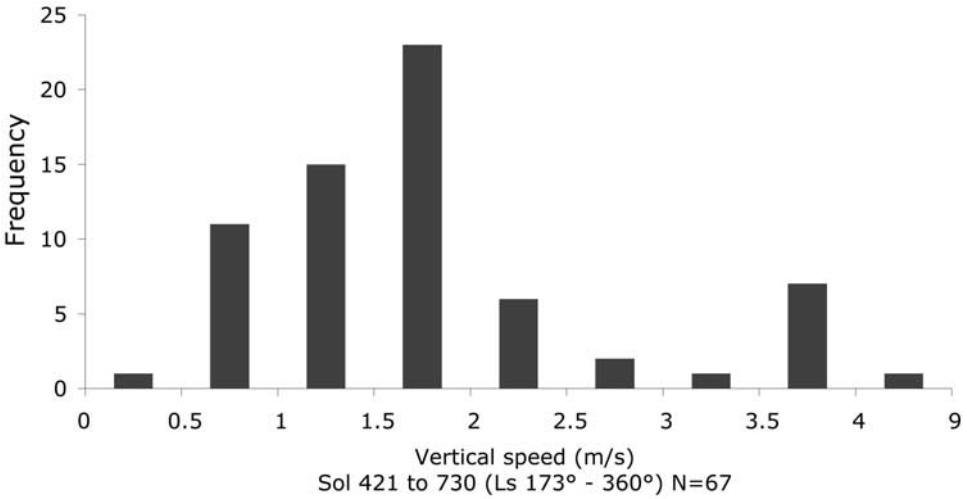

Figure 14. Distribution of vertical speeds within active dust devils for 67 cases.

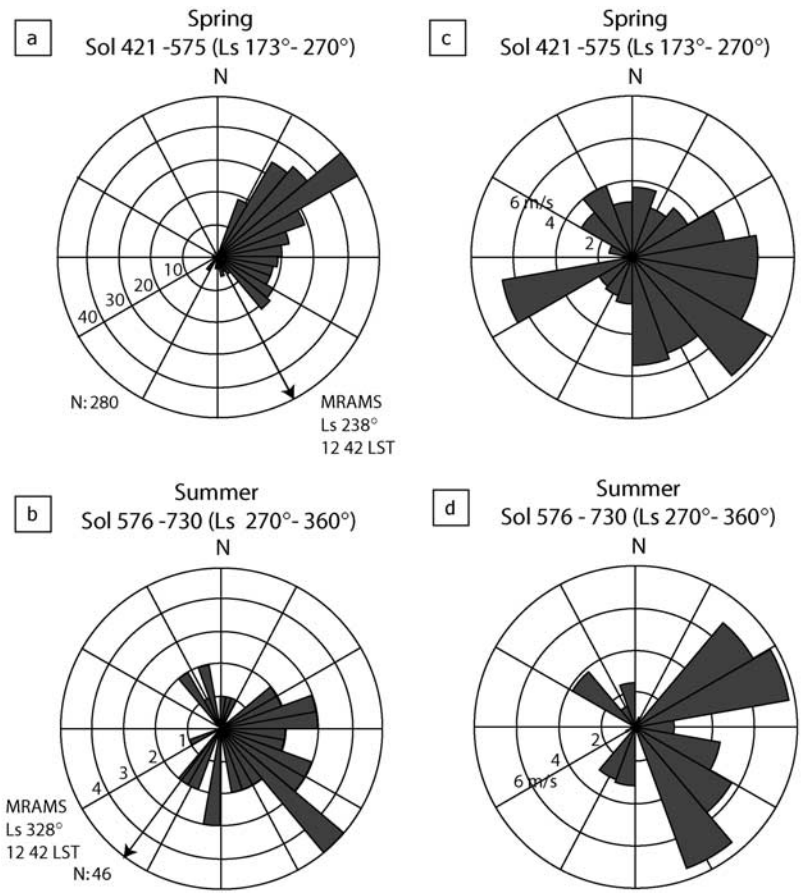

Figure 15. Characteristics of dust devils in Gusev crater for spring and summer: downwind azimuth directions (a) for the spring compared to (b) directions in the summer with concentric circles indicating the number of observations (a total of 280 observations, N, were obtained in the spring, compared to 46 in the summer). Arrows indicate prevailing downwind directions predicted by the Mars Regional Atmospheric Modeling System [*Rafkin et al.*, 2001] in the middle of the spring and summer seasons shortly after high noon, local solar time (LST). (c) Velocity vectors for the spring compared to (d) velocity vectors for the summer with concentric scales given in m/s.

observations were made over the entire ''doughnut'' shaped area constantly between the hours of 0930 and 1630. This value can then be divided by the total surface of the ''doughnut'' shaped area observed and by 236 sols (period of Navcam imaging), which equals about 50 active dust devils/km^2/sol, or 153,000 dust devils per sol for the total low-albedo zone. For an average flux of 2.07 10^{-5} this equals 3 kg/m^2/s; for the average duration of 170 s, this equals about 510 kg/m^2. In turn, the radius of the average dust devil is 6 m, giving a surface area of 113 m^2. This yields 5.8 10^4 kg/sol of dust raised during the 270 sol dust devil period over the low-albedo zone, or about 19 kg/km^2/sol. Assuming a dust density of 2600 kg/m^3 and a porosity of 50 percent, this mass would represent the removal of a uniform layer of dust about 4 micrometers thick over the entire low-albedo zone. However, as seen in Figure 3a, the overall low-albedo zone consists of dark tracks and higher albedo patches, suggesting that dust removal is not uniform over the entire surface (i.e., removal only along the dust devil paths). The ratio of tracks to nontrack areas is about 1:1, which would suggest removal of about 8 micrometers of dust from the surface.

[32] Although direct comparisons are difficult because of uncertainties in source area, this value is less than the estimate of *Pollack et al.* [1979] based on Viking data. They inferred a density for Martian dust of 3000 kg/m^3 and 50 percent pore space, and estimated the erosion in the source area for a typical dust storm of 200 microns. This value is for one dust storm, whereas our estimate for Gusev is for a full dust devil season. More recently, *Cantor et al.* [2001] estimated the amounts of dust in the atmosphere on the basis of the analysis of Mars Observer Camera images. For a typical regional dust storm, defined as 1.6 10^6 km^2 and lasting from 3 to 15 days, they estimated total dust loading of 2600 to 3600 kg/km^2, which yields a range of 173 to 1200 kg/km^2/sol. Our estimated dust loading from the low-albedo zone in Gusev crater is 19 kg/km^2/sol would suggest that dust devils make a small contribution to regional dust storms.

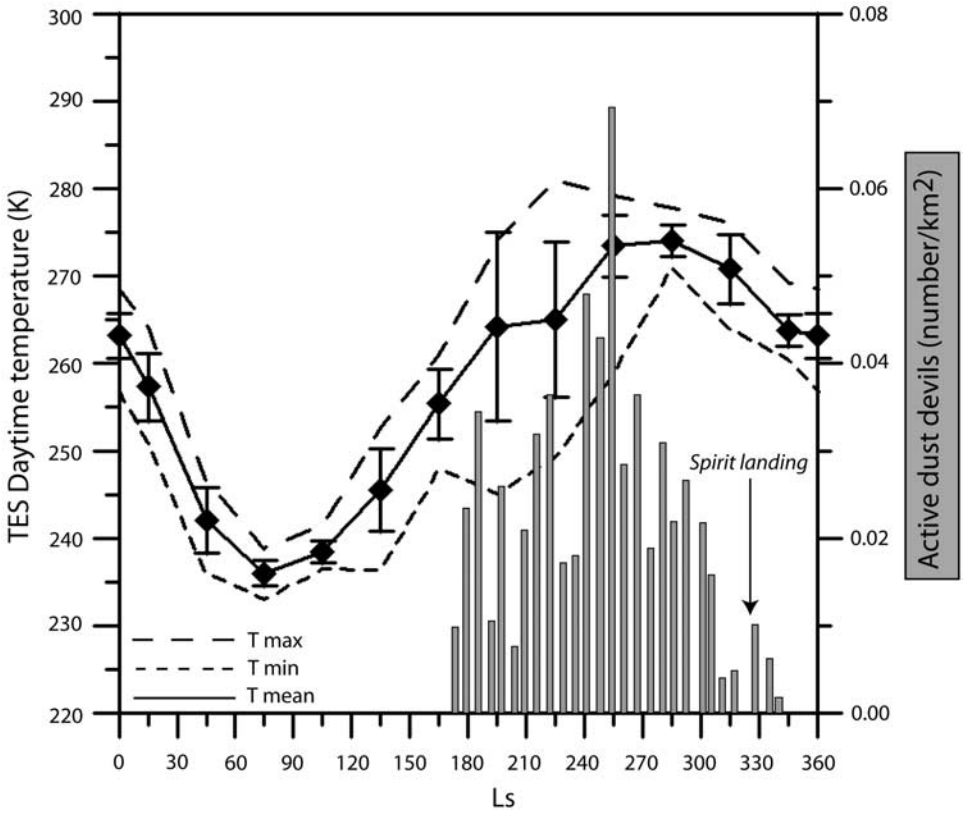

Figure 16. Daytime surface temperatures derived from Thermal Emission Spectrometer data on part of Gusev crater floor (28 February 1999 to 20 February 2005) and the density of active dust devils observed from Spirit plotted against L_s. Also shown is the time of landing of Spirit. Results suggest that the landing occurred in the waning stages of the dust devil "season," which appears to be governed at least partly by the surface temperature gradient.

[33] **Acknowledgments.** This work was performed for the Jet Propulsion Laboratory, California Institute of Technology, sponsored by the National Aeronautics and Space Administration. P. Whelley and S. Thompson were also supported by the NASA Space Grant Program at ASU and by the NASA Planetary Geology and Geophysics Program. We thank the NASA Space Photography Laboratory at ASU for use of some images used in this study. We thank C. Leovy and an anonymous reviewer for their thoughtful critique of the manuscript. All Spirit images can be found at the Analysis's Notebook: http://anserver1.eprsl.wustl.edu/.

References

Balme, M., and R. Greeley (2006), Dust devils on Earth and Mars, *Rev. Geophys.*, *44*, RG3003, doi:10.1029/2005RG000188.

Balme, M. R., P. L. Whelley, and R. Greeley (2003), Mars: Dust devil track survey in Argyre Planitia and Hellas Basin, *J. Geophys. Res.*, *108*(E8), 5086, doi:10.1029/2003JE002096.

Bell, J. F., III, and the Athena Science Team (2004), Pancam multispectral imaging results from the Spirit rover at Gusev Crater, Mars, *Science*, *305*, 800–806, doi:10.1126/science.3050794.

Biener, K. K., P. E. Geissler, A. S. McEwen, and C. Leovy (2002), Observations of dust devils in MOC wide angle camera images, *Lunar Planet. Sci.* [CD-ROM], *XXXIII*, abstract 2004.

Cantor, B. A., P. B. James, M. Caplinger, and M. J. Wolff (2001), Martian dust storms: 1999 Mars Orbiter Camera observations, *J. Geophys. Res.*, *106*(E10), 23,653–23,688.

Christensen, P. R., et al. (2001), Mars Global Surveyor Thermal Emission Spectrometer experiment: Investigation description and surface science results, *J. Geophys. Res.*, *106*(E10), 23,823–23,872.

Edgett, K. S., and M. C. Malin (2000a), New views of Mars eolian activity, materials, and surface properties: three vignettes from the Mars Global Surveyor Orbiter camera, *J. Geophys. Res.*, *105*, 1623–1650.

Edgett, K. S., and M. C. Malin (2000b), Martian dust raising and surface albedo controls: Thin, dark (and sometimes bright) streaks and dust devils in MGS high-resolution images, *Lunar Planet. Sci.* [CD-ROM], *XXXIII*, abstract 1073.

Ferri, F., P. H. Smith, M. Lemmon, and N. O. Rennó (2003), Dust devils as observed by Mars Pathfinder, *J. Geophys. Res.*, *108*(E12), 5133, doi:10.1029/2000JE001421.

Fisher, J. A., M. I. Richardson, C. E. Newman, M. A. Szwast, C. Graf, S. Basu, S. P. Ewald, A. D. Toigo, and R. J. Wilson (2005), A survey of Martian dust devil activity using Mars Global Surveyor Mars Orbiter Camera images, *J. Geophys. Res.*, *110*, E03004, doi:10.1029/2003JE002165.

Foley, D. J., P. L. Whelley, R. Greeley, and L. D. V. Neakrase (2005), Dust devil tracks on Mars: Observation and analysis from orbit and the surface, *Lunar Planet. Sci.* [CD-ROM], *XXXVI*, abstract 1162.

Grant, J. A., and P. A. Schultz (1987), Possible tornado-like tracks on Mars, *Science*, *237*, 883–885.

Greeley, R., M. R. Balme, J. D. Iversen, S. Metzger, R. Mickelson, J. Phoreman, and B. White (2003), Martian dust devils: Laboratory simulations of particle threshold, *J. Geophys. Res.*, *108*(E5), 5041, doi:10.1029/2002JE001987.

Greeley, R., et al. (2004), Wind-related processes detected by the Spirit rover at Gusev Crater, Mars, *Science*, *305*, 810–813, doi:0.1126/science.1100108.

Greeley, R., et al. (2005), Martian variable features: New insight from the Mars Express Orbiter and the Mars Exploration Rover Spirit, *J. Geophys. Res.*, *110*, E06002, doi:10.1029/2005JE002403.

Greeley, R., et al. (2006), Gusev crater: Wind-related features and processes observed by the Mars Exploration Rover Spirit, *J. Geophys. Res.*, *111*, E02S09, doi:10.1029/2005JE002491.

Herkenhoff, K. E., et al. (2004), Textures of the Soils and Rocks at Gusev Crater from Spirit's Microscopic Imager, *Science*, *305*, 824–826.

Ives, R. L. (1947), Behavior of dust devils, *Bull Am. Meteorol. Soc.*, *28*, 168–174.

Landis, G. A., K. Herkenhoff, R. Greeley, S. Thompson, P. Whelley, and the MER Athena Science Team (2006), Dust and sand deposition on the MER solar arrays as viewed by the Microscopic Imager, *Lunar Planet. Sci.*, *XXXVII*, abstract 1932.

Lemmon, M. T., et al. (2004), Atmospheric imaging results from the Mars Exploration Rovers: Spirit and Opportunity, *Science*, *306*, 1753–1756.

Leovy, C. B. (2003), Mars: The devil is in the dust, *Nature*, *424*, 1008–1009, doi:10.1038/4241008a.

Lugt, H. J. (1983), *Vortex Flow in Nature and Technology*, John Wiley, Hoboken, N. J.

Maki, J. N., et al. (2003), Mars Exploration Rover Engineering Cameras, *J. Geophys. Res.*, *108*(E12), 8071, doi:10.1029/2003JE002077.

Malin, M. C., and K. S. Edgett (2001), Mars Global Surveyor Mars Orbiter Camera: Interplanetary cruise through primary mission, *J. Geophys. Res.*, *106*(E10), 23,429–23,570.

Metzger, S. M. (1999), Dust devils as aeolian transport mechanisms in southern Nevada and in the Mars Pathfinder landing site, Ph. D. Thesis, Univ. of Nev., Reno.

Metzger, S. M. (2001), Recent advances in understanding dust devil processes and sediment flux on Earth and Mars, *Lunar Planet. Sci.* [CD-ROM], *XXXII*, abstract 2157.

Metzger, S. M. (2005), Evidence of dust devil scour at the MER Spirit Gusev site, *Lunar Planet. Sci.* [CD-ROM], *XXXVI*, abstract 2397.

Metzger, S. M., J. R. Carr, J. R. Johnson, M. Lemmon, and T. J. Parker (1998a), Dust devil vortices identified in the Mars Pathfinder camera images, *Bull. Am. Astron. Soc.*, *30*, Abstract 1023.

Metzger, S. M., J. R. Carr, J. R. Johnson, M. Lemmon, and T. J. Parker (1998b), Dust devil vortices identified in the Mars Pathfinder camera images: Exploring the land-atmosphere link, *Eos Trans. AGU*, *79*(45), Fall Meet. Suppl., F537.

Metzger, S. M., J. R. Johnson, J. R. Carr, T. J. Parker, and M. Lemmon (1999), Dust devil vortices seen by the Mars Pathfinder Camera, *Geophys. Res. Lett.*, *26*, 2781–2784.

Metzger, S. M., J. R. Carr, J. R. Johnson, M. Lemmon, and T. J. Parker (2000), Techniques for identifying dust devils in Mars Pathfinder images, *IEEE Trans. Geosci. Remote Sens.*, *38*, 870–876.

Murphy, R. J., and S. Nelli (2002), Mars Pathfinder convective vortices: Frequency of occurrence, *Geophys. Res. Lett.*, *29*(23), 2103, doi:10.1029/2002GL015214.

Neubauer, F. M. (1966), Thermal convection in the Martian atmosphere, *J. Geophys. Res.*, *71*, 2419–2426.

Pollack, J. B., D. S. Colburn, F. M. Flasar, R. Kahn, C. E. Carlston, and D. Pidek (1979), Properties and effects of dust particles suspended in the Martian atmosphere, *J. Geophys. Res.*, *84*(B6), 2929–2945.

Rafkin, S. C. R., and T. I. Michaels (2003), Meteorological predictions for 2003 Mars Exploration Rover high-priority landing sites, *J. Geophys. Res.*, *108*(E12), 8091, doi:10.1029/2002JE002027.

Rafkin, S. C. R., R. M. Haberle, and T. I. Michaels (2001), The Mars Regional Atmospheric Modeling System: Model description and selected simulations, *Icarus*, *151*, 228–256.

Rennó, N. O., M. L. Burkett, and M. P. Larkin (1998), A simple thermodynamical theory for dust devils, *J. Atmos. Sci.*, *55*, 3244–3252.

Rennó, N. O., A. A. Nash, J. Lunine, and J. Murphy (2000), Martian and terrestrial dust devils: Test of a scaling theory using Pathfinder data, *J. Geophys. Res.*, *105*(E1), 1859–1866.

Ringrose, T. J., and J. C. Zarnecki (2002), Martian and terrestrial dust devils, *Lunar Planet. Sci.* [CD-ROM], *XXXIII*, abstract 1183.

Ringrose, T. J., M. C. Towner, and J. C. Zarnecki (2003), Convective vortices on Mars: A reanalysis of Viking Lander 2 meteorological data, sols 1–60, *Icarus*, *163*, doi:10.1016/S0019-1035 (03)00073-3.

Rossi, A. P. (2002), Possible dust devils tracks detected in Tenere' Desert, (Niger): An analogue to Mars, *Lunar Planet. Sci.* [CD-ROM], *XXXIII*, abstract 1307.

Rossi, A. P., and L. Marinangeli (2004), The first terrestrial analogue to Martian dust devil tracks found in Ténéré Desert, Niger, *Geophys. Res. Lett.*, *31*, L06702, doi:10.1029/2004GL019428.

Ryan, J. A., and R. D. Luchich (1983), Possible dust devil vortices on Mars, *J. Geophys. Res.*, *88*, 11,005–11,011.

Sagan, C., and J. B. Pollack (1969), Windblown dust on Mars, *Nature*, *223*, 791–794.

Sagan, C., J. Veverka, and P. Gierasch (1971), Observational consequences of Martian wind regions, *Icarus*, *22*, 24–47.

Schofield, J. T., J. R. Barnes, D. Crisp, R. M. Haberle, S. Larsen, J. A. Magalhães, J. R. Murphy, A. Seiff, and G. Wilson (1997), The Mars Pathfinder atmospheric structure investigation/meteorology (ASI/MET) experiment, *Science*, *278*, 1752–1758.

Sinclair, P. C. (1969), General characteristics of dust devils, *J. Appl. Meteorol.*, *8*, 32–45.

Sinclair, P. C. (1973), The lower structure of dust devils, *J. Atmos. Sci.*, *30*, 1599–1619.

Smith, P. H., and M. T. Lemmon (1999), Opacity of the Martian atmosphere measured by the imager for Mars Pathfinder, *J. Geophys. Res.*, *104*, 8975–8986.

Squyres, S. W., and the Athena Science Team (2004), The Spirit Rover's Athena science investigation at Gusev Crater, Mars, *Science*, *305*, 794–799, doi:10.1126/science.3050794.

Squyres, S. W., et al. (2003), Athena Mars rover science investigation, *J. Geophys. Res.*, *108*(E12), 8062, doi:10.1029/2003JE002121.

Sutton, J. L., C. B. Leovy, and J. E. Tillman (1978), Diurnal variations of the Martian surface layer meteorological parameters during the first 45 sols at two Viking lander sites, *J. Atmos. Sci.*, *35*, 2346–2355.

Thomas, P., and P. G. Gierasch (1985), Dust devils on Mars, *Science*, *230*, 175–177.

Tomasko, M. G., L. R. Doose, M. Lemmon, P. H. Smith, and E. Wegryn (1999), Properties of dust in the Martian atmosphere from the Imager on Mars Pathfinder, *J. Geophys. Res.*, *104*(E4), 8987–9008.

R. E. Arvidson, Department of Earth and Planetary Sciences, Washington University in St. Louis, St. Louis, MO 63130, USA. (arvidson@wunder.wustl.edu)

N. A. Cabrol, NASA Ames Research Center, MS 245-3, Moffett Field, CA 94035-1000, USA. (ncabrol@mail.arc.nasa.gov)

D. J. Foley, R. Greeley, L. D. V. Neakrase, and P. L. Whelley, School of Earth and Space Exploration, Arizona State University, Box 871404, Tempe, AZ 85287-1404, USA. (greeley@asu.edu)

B. J. Franklin and M. P. Golombek, Jet Propulsion Laboratory, 4800 Oak Grove Drive, MS 183-501, Pasadena, CA 91109, USA. (brenda.franklin@jpl.nasa.gov; mgolombek@jpl.nasa.gov)

P. G. Geissler, Astrogeology Program, U.S. Geological Survey, 2255 North Gemini Drive, Flagstaff, AZ 86001, USA. (pgeissler@usgs.gov)

R. O. Kuzmin, Vernadsky Institute, Russian Academy of Sciences, Kosygin Str 19, Moscow 117975 GSP-1, Russia. (rok@geokhi.ru)

G. A. Landis, NASA Glenn Research Center, 21000 Brookpark Road, Cleveland, OH 44135, USA. (geoffrey.a.landis@nasa.gov)

M. T. Lemmon, Department of Atmospheric Sciences, Texas A&M University, College Station, TX 77843-3150, USA. (lemmon@neo.tamu.edu)

S. W. Squyres, Department of Astronomy, Cornell University, 428 Space Sciences Building, Ithaca, NY 15853-1301, USA. (squyres@astro.cornell.edu)

S. D. Thompson, Department of Geological Sciences, University of Nevada at Reno, MS 172, Reno, NV 89557-0138, USA.